Sensing and Bio-Sensing Research 43 (2024) 100619

Contents lists available at ScienceDirect

Sensing and Bio-Sensing Research

journal homepage: www.elsevier.com/locate/sbsr

Study of the evolution in space and time of water diffusion in a leaf through a sub-terahertz portable imaging system

F.V. Di Girolamo [a,b], R. Paoletti [a,d], A. Tredicucci [b,c,e], A. Toncelli [a,b,c,e,*]

[a] Istituto Nazionale di Fisica Nucleare, Sezione di Pisa, Largo B. Pontecorvo 3, 56127 Pisa, Italy
[b] Dipartimento di Fisica "E. Fermi", Università di Pisa, Largo B. Pontecorvo 3, 56127 Pisa, Italy
[c] Istituto Nanoscienze – CNR, Piazza S. Silvestro 12, Pisa 56127, Italy
[d] Dipartimento di Scienze Fisiche, della Terra e dell'Ambiente, Sezione di Fisica, Università di Siena, via Roma 56, 53100 Siena, Italy
[e] Centro per l'Integrazione Della Strumentazione Dell'Università di Pisa (CISUP), Lungarno Pacinotti 43/44, 56126 Pisa, Italy

ARTICLE INFO

Keywords:
Terahertz
Living samples
Videos data
Water diffusion

ABSTRACT

Among the non-destructive techniques capable of obtaining information on biological systems even *in vivo*, terahertz-based techniques are emerging due to their specificity to the water content, which can represent an important indicator of the presence of microorganisms and, in general, of the health status, particularly in plants. Nevertheless, the analysis of the extracted data (especially for images) and the exploitation of the potential of the technique for the study of the complex phenomena that occur in living tissues are still almost unexplored fields. In this work, the hydration status of leaves both *in vivo* and *ex vivo* was monitored continuously and non-destructively by acquiring videos in the sub-terahertz range through a portable imaging system. A model for describing the water flow in space and time in the midvein of a leaf is obtained which is suitable for the analysis of the data extracted from the portable sub-terahertz imaging system. These results show that terahertz-based technology can be used to study biological phenomena even *in vivo*; moreover, they pave the way for the introduction of a general method for the analysis of terahertz data based on surface fits in space and in time as well.

1. Introduction

The Terahertz (THz) frequency range is usually defined as the region in between 0.1 and 10 THz and is sandwiched between infrared and microwaves. The analysis of data obtained using THz-based techniques has already demonstrated its potential in obtaining significant information on the health status of biological samples, information that would otherwise not be easily accessible with other techniques [1–6]. Moreover, THz radiation is non ionizing and non-destructive [7] and it is particularly sensitive to polar molecules such as water [8]: in fact, it has already been demonstrated that the attenuation of the signal transmitted by living bodies in the THz range is directly related to the water content in the sample [9,10]. Furthermore, the proportionality of THz attenuation with water content in both *in-vivo* and *ex-vivo* leaves has been extensively evaluated [11–21] and water content has been found to be closely related to leaf health [22].

Despite the initial difficulties encountered in the realization of emitters and detectors in the THz range, nowadays several devices and techniques [6–8] have been developed and assessed for many applications. Compared to microwaves, THz techniques have the advantage of being specifically sensitive to water and also to biological molecules such as nucleobase and amino acids [23]. The infrared region is also widely used for non-destructive monitoring of biological samples since it senses intramolecular vibrations and rotations, but, given its shorter wavelength, the infrared signal is more strongly affected by scattering problems and is less sensitive to the water content [23].

Among all different THz techniques, the main distinction can be drawn between continuous (CW) wave and pulsed time domain (TD) approaches [6–8]. Time domain techniques rely on the generation of pulsed radiation that can be sampled in time and can thus be used for spectroscopy *via* Fourier transform. In this case, imaging can be achieved by scanning the sample across the cross-section of the beam, but this makes it a slow technique that cannot be used in real time.

CW techniques, on the other hand, are based on the emission of a continuous terahertz beam; they are generally characterized by narrow linewidth, short response time and high available power, this leads to a

* Corresponding author at: Dipartimento di Fisica "E. Fermi", Università di Pisa, Largo B. Pontecorvo, 3, 56127 Pisa, Italy.
E-mail address: alessandra.toncelli@unipi.it (A. Toncelli).

https://doi.org/10.1016/j.sbsr.2024.100619
Received 22 August 2023; Received in revised form 23 December 2023; Accepted 29 January 2024
Available online 30 January 2024

larger penetration depth and a better signal-to-noise-ratio. Moreover, CW systems can be used in conjunction with a camera for real-time applications [10,11] and are usually more compact than time-domain setups and can also be made portable for their use outside the laboratory, directly in the fields. A direct consequence of the relationship between THz intensity and water concentration [9,10], is that THz signals are more attenuated if the water content is higher and *vice versa*. This finding has been widely exploited for the assessment of the health status of biological samples with both TD and CW THz imaging, for example by comparing water content in unhealthy and healthy samples [2–4,6,23]. Furthermore, the use of a CW imaging system allows obtaining information regarding the water content in the different leaf compartments, which can be useful both for the study of plant physiology and for the early detection of pathogens [6].

A more in-depth study of water management in living organisms cannot be limited to the simple spatial mapping of the water resource but must also involve the study of its diffusion in tissues and cells. [24]. Diffusion is characterized by the variation of water content over both space and time; therefore, video acquisition gives the obvious advantage of providing detailed information on the water content change in time and space without destroying the sample. Water diffusion in a leaf involves several phenomena simultaneously and presents serious problems for analytical modelling. For example, hydration in a leaf *in-vivo* occurs over a few hours and this presents issues related to the difficulty of keeping all other parameters constant and, consequently, to their inclusion in the model. In contrast, hydration of the removed leaf begins immediately after introducing the stalk into the syringe and occurs within a few minutes, which makes the analysis much easier. Moreover, the spatial evolution of the water content at a random point in the leaf tissue, for example, can occur in any direction, depending, for instance, on the direction of the vein through which water is brought to the cells. To deal with these issues, this study was conducted on an *ex-vivo* leaf and the analysis focused on the middle vein because the "macroscopic" direction of the water flow can be assumed to coincide with the axis of the midvein and because this is the central region of the leaf that should be least sensitive to stretching. The results were fitted with a model derived starting from Fick's diffusion law which has already been proposed to model the diffusion of water in cells and tissues [24,25].

Furthermore, here we also present a case study on both the continuous monitoring of hydration and dehydration dynamics in leaf compartments *in-vivo* and *ex-vivo* and the study of water diffusion through quantitative analysis of the spatial-temporal THz video acquisition of a leaf during hydration and dehydration.

2. Materials and methods

The terahertz imaging system (Fig. 1a and b) was composed of an impact avalanche transit time (IMPATT) diode source (IMPATT-100-H/F, output 80 mW at 100 GHz, Terasense, San Jose, USA) with a slightly diverging beam and a THz camera (Tera-1024 32 × 32, Terasense, San Jose, USA) made of a square matrix of sensors (1024 pixel; pixel size 1.5 mm; sensitivity 50 kV/W). This device is capable of recording both single pictures and continuous videos and has already been used on other biological samples [5,6]. The distance between the diode source and the THz camera was about 40 cm. This distance was optimized to have the most uniform illumination possible in the detector array area. Moreover, the exposure time of the image was optimized to avoid saturation of the pixel signal.

Measurements of the THz transmission during hydration and dehydration were recorded in both removed (*ex vivo*) and attached (*in vivo*) leaves of sage, *Salvia Officinalis*. During the measurements, the leaf was placed outstretched on the camera and held as fixed as possible with scotch tape.

In the case of the removed leaf, water was supplied to the leaf by immersing the stalk in a syringe without a needle and filled with water [5]. The measurement of the THz transmission in hydration began immediately after the leaf was put in contact with water and lasted about 2500 s. The results obtained for hydration *ex vivo* were taken as a reference because phenomena that can occur for instance in the entire plant or for longer response times (such as phenomena due to plant segments, soil) can be reasonably neglected. In the case of an attached leaf, water was supplied by irrigating the entire plant; the measurement lasted $2.5*10^5$ s (approximately three days) after irrigation. The plant was put close to the imaging system; only one leaf was placed between the source and the detector and kept outstretched and in fixed position as much as possible, even if a few leaf movements have occurred during the observation time. Water was supplied in the late morning (about 11 a.m.) after approximately 18 h without irrigation both for the removed and attached leaves; hydration was performed under artificial room light while dehydration was performed in the dark. The leaves were chosen to be of comparable size.

Once the videos were acquired, in-house software programs based on appropriate Matlab functions were used to extract individual frames and perform image data analysis. The same software was used to identify leaf borders but also the main parts of the leaf, in particular the midvein [5], either to select it or to exclude it from the analysis.

According to the Lambert-Beer law, the absorbance of a radiation travelling in a non-scattering medium is proportional to the optical

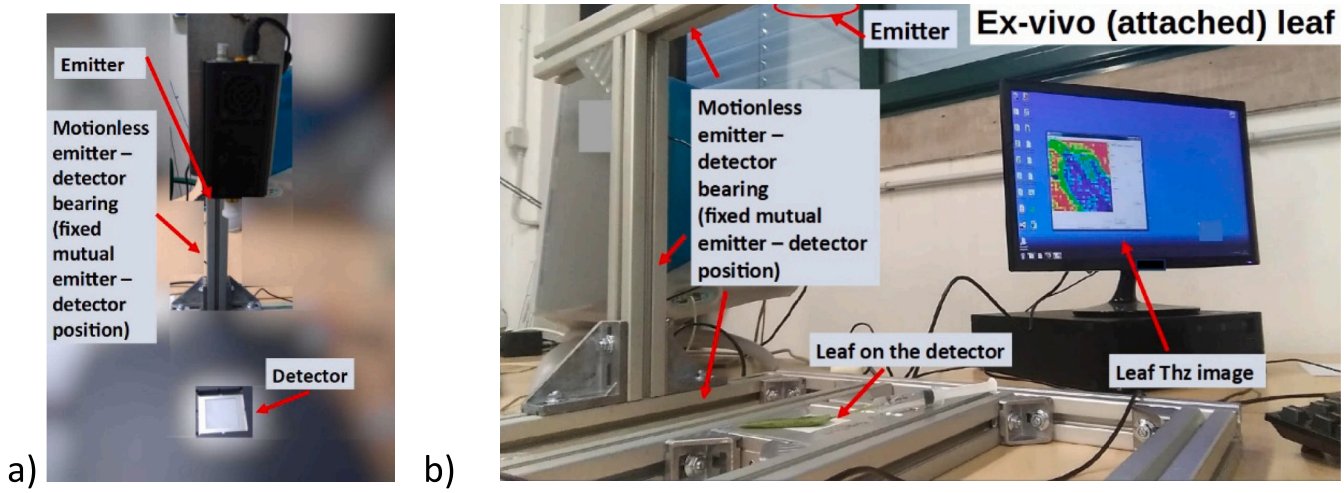

Fig. 1. a) Terahertz measurement setup. b) *Ex vivo* neasurement, with removed leaf on the camera with syringe providing water. A figure of *in vivo* measurement is reported in the S.I.. See also [5,6] for more information on the THz measurement setup.

thickness travelled [24]. In analogy to this, the attenuation matrix was calculated as the absorbance of each pixel for the entire image data (32 × 32 matrix of intensity values) of each frame *via* the following equation:

$$A(i,j) = -ln\frac{I_{(i,j)}}{I_{blank(i,j)}} \quad (1)$$

where $I_{blank(i,j)}$is the background data acquired without leaf and measured by the pixel sensor, and $I_{(i,j)}$ is the signal transmitted by the leaf in the selected region and measured by the pixel sensor.

In Fig. 2 some steps of the above calculation are shown. In detail, image 2a has been obtained by performing the ratio $\frac{I_{(i,j)}}{I_{blank(i,j)}}$ over each pixel, image 2b by performing $-ln\left(\frac{I_{(i,j)}}{I_{blank(i,j)}}\right)$ over each pixel.

The perimeters of the primary vein and the external region of the midvein region were determined using appropriate edge recognition functions on the attenuation image. An example is shown in Fig.2d: the perimeters of the midvein region and of the leaf region surrounding the midvein are highlighted with red and blue lines, respectively.

It is worth mentioning that, in order to determine the "most likely" attenuation for a specific region (entire leaf, midvein, leaf outside midvein), the histogram and the subsequent of the normal distribution were extended to the intensity values corresponding to pixels within the considered region.

3. Experimental results and discussion

3.1. Ex vivo and in vivo mean hydration versus time

Kim and co-workers [26] reported in the near – infrared range a shift of the data matrix distribution towards higher values between a dried leaf image and a fresh leaf image. Starting from a similar procedure, here the histogram of the attenuation matrix (extended over the specific region considered) was fitted by a normal distribution and the attenuation value corresponding to the mean of the distribution was determined. Hydration and dehydration curves were then obtained by plotting the attenuation values as a function of time. Taking the results of *ex vivo* hydration as a reference, it is possible to state that an increase in the attenuation value can be associated with an increase in the water content in the leaf and thus to hydration. It is worth mentioning that a shift towards higher attenuation is accompanied by an increase of the standard deviation of the distribution (at least in *ex vivo* results).

The attenuation obtained as described above was plotted as a function of time; The results are shown in Fig. 3. With the aim of identifying one or more functions which could model the curves in Fig.3, some results reported in the literature were taken into consideration. Gente and Koch [13] used an exponential function (after Kinder et al. [27]) to fit the terahertz transmission monitoring water status in a coffee plant deprived from water. Castro-Camus et al. [12] fitted the stomatal conductance after the application of abscisic acid (which induces stomatal closure and thus an increase in water) with a double exponential.

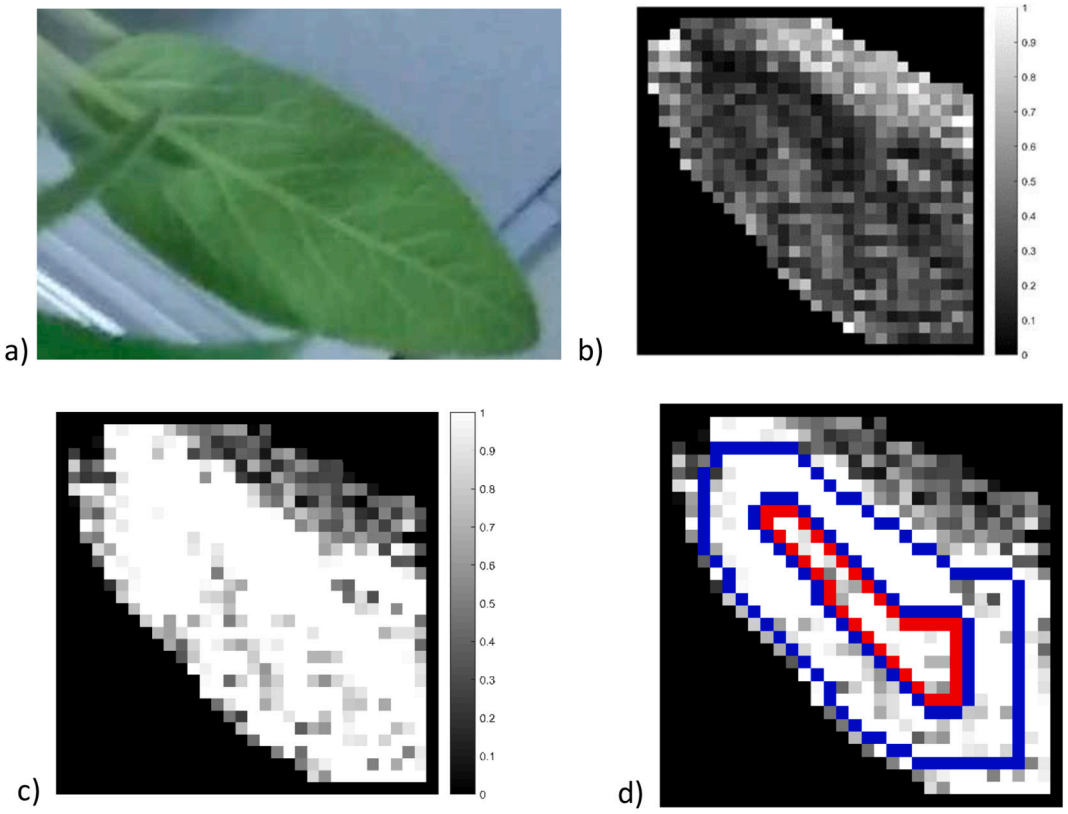

Fig. 2. Examples of attenuation images. a) Optical image of the leaf measured *in vivo*. b) Intensity data with leaf divided by the original data without leaf ($\left(\frac{I_{(i,j)}}{I_{blank(i,j)}}\right)$). c) The image obtained by performing the minus logarithm of the data of image 2a ($-ln\left(\frac{I_{(i,j)}}{I_{blank(i,j)}}\right)$). d) The contours of the leaf and midvein areas are superimposed to image 2c ($-ln\left(\frac{I_{(i,j)}}{I_{blank(i,j)}}\right)$). The red and blue lines respectively highlight the perimeters of the midvein region and of the region of the leaf outside the midvein. In the figure b) pixel value is lower where the signal is more attenuated (*i.e.* $I_{(i,j)}$ is lower and $0<\left(\frac{I_{(i,j)}}{I_{blank(i,j)}}\right)<1$); in figure c) and d), instead, pixel value is higher when the signal is more attenuated because ($-ln\left(\frac{I_{(i,j)}}{I_{blank(i,j)}}\right)$) for $0<\left(\frac{I_{(i,j)}}{I_{blank(i,j)}}\right)<1$ is a decreasing function. (For interpretation of the references to colour in this figure legend, the reader is referred to the web version of this article.)

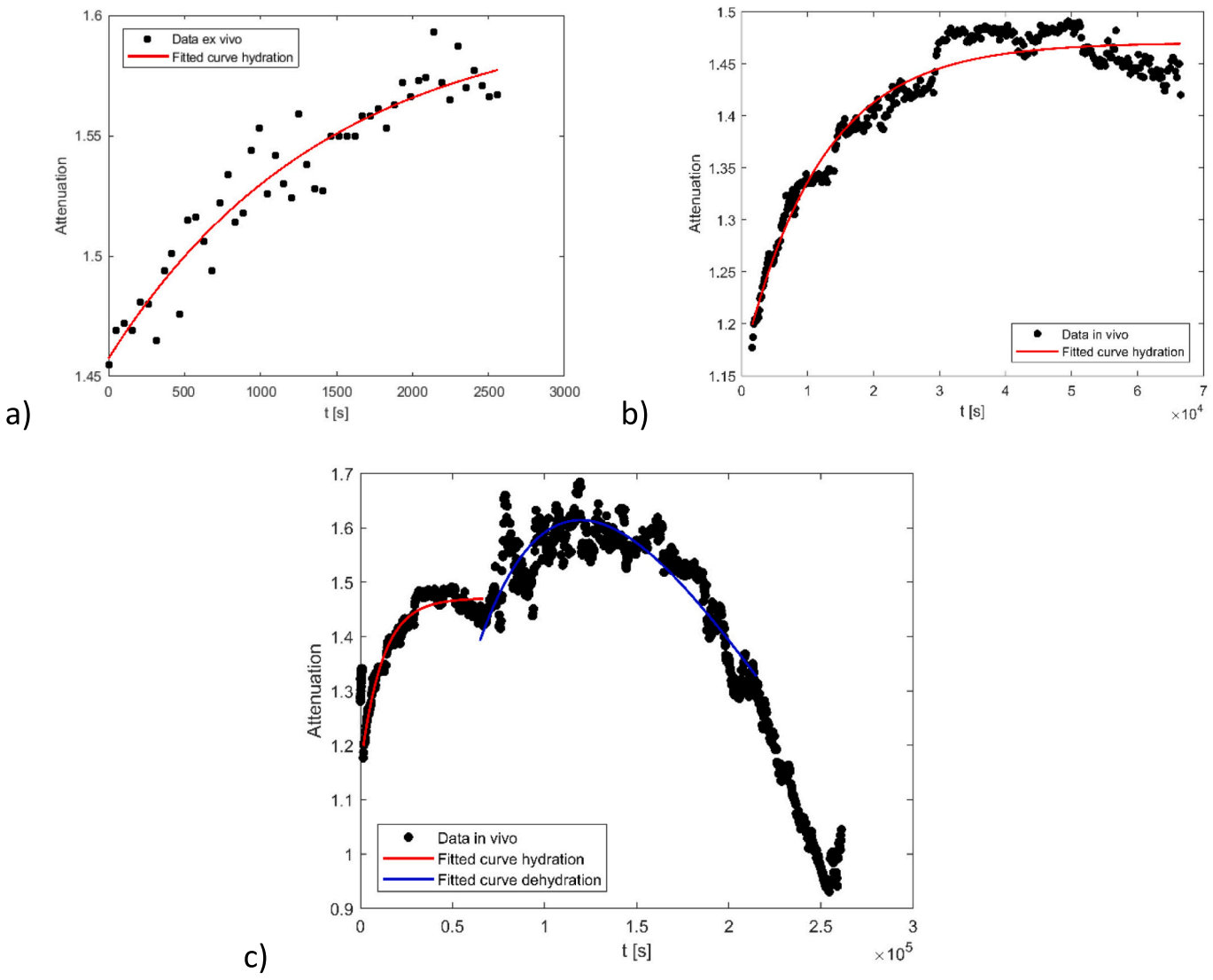

Fig. 3. Attenuation *versus* time curves during hydration/dehydration *in vivo* and *ex vivo*. (a) *Ex vivo* hydration dynamics, fitted with eq. (2). (b) *In vivo* hydration curve, fitted with eq. (2). (b) *In vivo* complete hydration- dehydration curve, fitted with eq. (2) for hydration and eq. (3) for dehydration. The procedure used for the determination of leaf area (parameters of edge function such as threshold and morphological operations) is the same for a) and b).

Exponential functions have been also used to fit water uptake by roots [28], while the flow of water through/across a plant segment (or the entire plant) is given by the water potential difference driving the flow divided by the hydraulic resistance of the plant segment (or the whole plant) [29].

In this case, the hydration dynamics have been fitted by the following exponential function (more details are reported in the Supplementary Information):

$$y_h(t) = y_0 - Ae^{(-k_b t)} \tag{2}$$

where the parameters can be tentatively interpreted as follows: y_0 is a quantity proportional to the leaf water potential at the turgor loss point, related to the maximum leaf water content [21,30]; A is a constant related to the diffusion of water into the plant or plant segment and k_b is related to the timescale of the chemical reactions taking place in the leaf.

Instead, it was found that the dynamics of dehydration is well fitted by the following exponential function (more details are given in the Supplementary Information):

$$y_d(t) = \frac{N_0}{k_b - (2k_0^2)}\left[e^{-(2k_0^2)t} - e^{-k_b t}\right] \tag{3}$$

where $k_0{}^2$ is the water diffusion timescale; k_b is the chemical reaction timescale; N_0 is a constant related to the maximum water concentration in the midvein.

Results are presented in Fig. 3 a and b for *ex vivo* and *in vivo* experiment, respectively, and fitting parameters are reported in Table 1 for hydration and in Table 2 for dehydration.

In the case of the removed leaf, the attenuation increases exponentially immediately after water supply, suggesting an increase in water content (Fig.3a). This agrees well with the literature, where a similar behaviour has been ascribed to the hydration dynamics [12,31].

In the case of attached leaf (Fig.3b and c), the attenuation increases

Table 1
Fitting parameters for *ex vivo* and *in vivo* hydration range (with 95% confidence bounds).

	y_0	A	k_b (10^{-4} s^{-1})	R^2
Removed Leaf, *ex vivo* (hydration)	1.601 ± 0.028	0.14 ± 0.02	6.7 ± 2.9	0.91
Attached Leaf, *in vivo* (hydration)	1.470 ± 0.003	0.31 ± 0.01	0.8 ± 0.5	0.95

Table 2
Fitting parameters for *in vivo* dehydration range (with 95% confidence bounds).

	k_0^2 (10^{-6} s^{-1})	k_b (10^{-6} s^{-1})	N_0 (10^{-5})	R^2
Attached Leaf, *in vivo* (dehydration)	6.1 ± 0.8	5.5 ± 0.9	7.5 ± 0.2	0.78

rapidly immediately after plant watering, then it slows down and finally decreases again suggesting that dehydration begins to occur. An exponential growth regime can be identified soon after plant watering (Fig.3b), which can also be attributed to the hydration dynamics. This behaviour was fitted with Eq. (2) and the fitting parameters are reported in Table 1. Eventually, an exponential decay regime (Fig.3c) follows, that can be consequently interpreted as dehydration dynamics [13]. This behaviour was fitted with eq. (3) and the fitting parameters are reported in Table 2.

The k_b parameter for *ex vivo* hydration is roughly eight times higher than the same parameter for *in vivo* hydration. As expected, this suggests that *in vivo* hydration is much slower than in the case of the removed leaf, which is explained by taking into account that for the whole plant the number of segments is obviously greater than for the single leaf, and so is the hydraulic resistance [29]. The parameter k_b for dehydration is about two orders of magnitude smaller than the same parameter for hydration. This, in agreement with the consistency between k_b and k_0^2 for dehydration, suggests that during dehydration the speed of the chemical reaction is strongly determined by the speed of the water flow: in this condition, water is in short supply and, without water, chemical reactions cannot occur. This could also suggest that the plant tends to retain water during drought periods, as also found in the literature [30,32].

The phenomena that occur in plants during drought are the subject of intensive study [30,32]. The opinions regarding the relationship between the available soil water content and the leaf water content converge towards two main schools of thought, depending on the differences in the effects of soil water on plant growth during drought [32]. In particular, it is still debated whether or not the soil water availability depends linearly on the soil water content or not; plant water content is not always linearly dependent on available soil water content [32].

Another point of discussion is represented by the presence of two or more domains in the pressure-volume curves: the third domain has usually been explained by a phenomenon of temporary accumulation of water in the apoplastic space [30]. This effect has sometimes been interpreted as an artefact of rehydration ("the plateau effect"), while Nguyen et al. instead have presented evidence to support the hypothesis that it may actually reflect the anatomical characteristics of the leaf. In particular, in a leaf there are different kinds of cells specialized in different functions; they may have different elasticity coefficient and thus different ability to maintain turgor during drought [30].

3.2. Evolution in space and time of the hydration flux in a leaf

In this study, a system as simple as possible was chosen as a case study for identifying a mathematical model suitable for surface fitting of terahertz data. One of the reasons why the choice fell on sage is its relatively small size and rather wide midvein, which guarantees a sufficiently large portion of the image in which the water flow can reasonably be considered quite uniformly occurring along the same direction (roughly parallel to the axis of the midvein, as illustrated in the drawing of Fig. 4 a and b and as will be explained in more details below and in the Supplementary Information). Figs. 4 a, b and c schematically illustrate some details of the experiment and are useful to understand some basic assumptions of the model. In Fig. 4a, it is possible to notice in a typical sage leaf the primary vein (or midvein), which starts from the end of the stalk and ends at the tip, and several (about 12–14) secondary veins that originate from the primary vein. In Fig. 4b it is possible to see how the sage leaf was placed on the sensor and the approximate extent of the midvein region; the reduction of the diameter of the midvein from the stalk to the tip is also visible.

In Fig. 4b it is possible to observe that the leaf was placed on the sensor so as to have the stalk in the upper-left corner of the image and the tip in the lower-right corner: the direction of the flow then results to be approximately coincident with the diagonal of a pixel. In order to further clarify this last point, in Fig. 4c a schematic zoom has been done on the initial part of the midvein: the squares represent the pixels, while the x axis represents approximately the direction of the main flow and the axis of the midvein.

In the development of the mathematical model, the first assumption that was made is that of a Newtonian flow [24]: taking into account Fig. 4b, it is possible to assume that, once y is fixed, the flow depends only on x and on time. Once this assumption had been made, it was possible to study the diffusion only as a function of x and time, for each y. In this treatment, any source of turbulence was neglected. Of course, these assumptions are expected to be less verified at the extremes of the midvein (*i.e.* y = 1 and y = 7) due to the reduction of the contribution of the midvein and to the presence of connections with the secondary veins. Under these conditions, the evolution of the water content in time and space can be described with a function ψ depending on space and time which, in general, can be obtained as an approximate solution of the diffusion equation [24,25]:

$$\frac{\partial \psi}{\partial t} = D\frac{\partial^2 \psi}{\partial x^2} \tag{4}$$

where D is the diffusion constant. In the presence of chemical reactions, this can be modified as [25] (see also Supplementary Information):

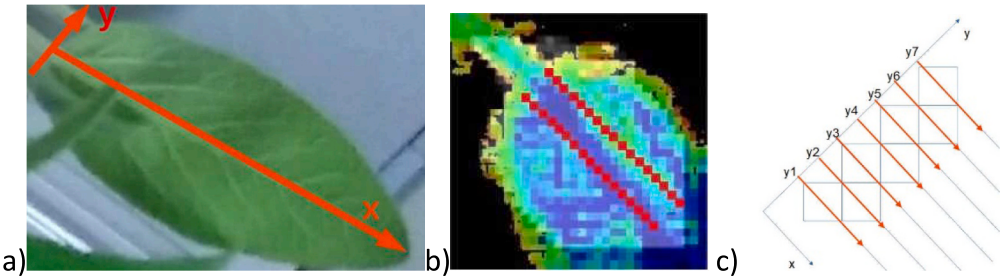

Fig. 4. (a)Schematic drawing of a sage leaf. The primary vein (midvein) is indicated, along with the most visible secondary veins (roughly 12–14) directly departing from the primary vein. (b) Modified image (from [1]) of a sage leaf in pixels as acquired by the sub-terahertz imaging system. The region delimited by the red squares approximately coincides with the midvein. The water flow comes from the stalk (upper left corner) to the tip (lower right corner). (c) Schematic zoom of the initial part of the midvein. The squares schematically represent the pixels of the image. The x axis has approximately the same direction of the midvein axis and also of the flow. It roughly coincides also with the diagonal of a pixel. The y axis roughly represents the direction of the diameter of the midvein. (For interpretation of the references to colour in this figure legend, the reader is referred to the web version of this article.)

$$\frac{\partial \psi^*}{\partial t} = D\frac{\partial^2 \psi^*}{\partial x^2} - k_{chem}\psi^* \tag{5}$$

where k_{chem} is related to the timescale of the chemical reactions and the asterisk is introduced to distinguish the solution with chemical reactions from the previous one.

Eq. 5 can be solved by defining the origin of the x axis as the starting point of the midvein, as illustrated in Fig. 4a, b and c and imposing boundary conditions $[H_2O] \simeq 0$ for $t = 0$. In this case, the following solution is obtained:

$$[H_2O] = \frac{C_0}{k_b} - \frac{C_0}{k_b}\, e^{-k_b t} + \frac{{k_1}^2 C_1 sin[k_1(x+\Delta x)\ ]}{{k_1}^2 + k_{chem}}\left[\frac{e^{-k_b t}}{k_b - \left({k_1}^2 + k_{chem}\right)}\right] + \frac{{k_2}^2 C_2 sin[k_2(x+\Delta x)\ ]}{{k_2}^2 + k_{chem}}\left[\frac{e^{-k_b t}}{k_b - \left({k_2}^2 + k_{chem}\right)}\right] - \frac{k_{chem} C_1 sin[k_1(x+\Delta x)\ ]}{{k_1}^2 + k_{chem}}\left[\frac{1 - e^{-k_b t}}{k_b}\right] - \frac{k_{chem} C_2 sin[k_2(x+\Delta x)\ ]}{{k_2}^2 + k_{chem}}\left[\frac{1 - e^{-k_b t}}{k_b}\right] \tag{6}$$

where C_0 is related to the water content at the stalk cut, C_1 and C_2 are related to the decrease of water content along x, k_1 and k_2 are related to the water diffusion along x, k_{chem} is related to the chemical rection timescale and Δx is related to the distance between the cut section of the stalk (where the boundary condition reported above actually holds) and the section where the midvein is assumed to begin. Further details are provided in the Supplementary Information.

Eq. (6) was used to fit the attenuation with respect to x and time in the midvein at y = y1, y = y2, y = y3, y = y4, y = y5, y = y6, y = y7 (see Fig. 4c and Supplementary Information). y = 1 and y = 7 approximately represent the edges of the midvein (bottom left and the top right red lines in Fig. 4c, respectively). As a consequence of the basic assumptions of the model fits are expected to be more reliable at the centre of the midvein which consequently assumed a more central role in the following discussion.

Here we report experimental results for y = 4 and corresponding fitting parameters, while a more detailed description of the fitting function, the complete experimental results and fitting parameters with

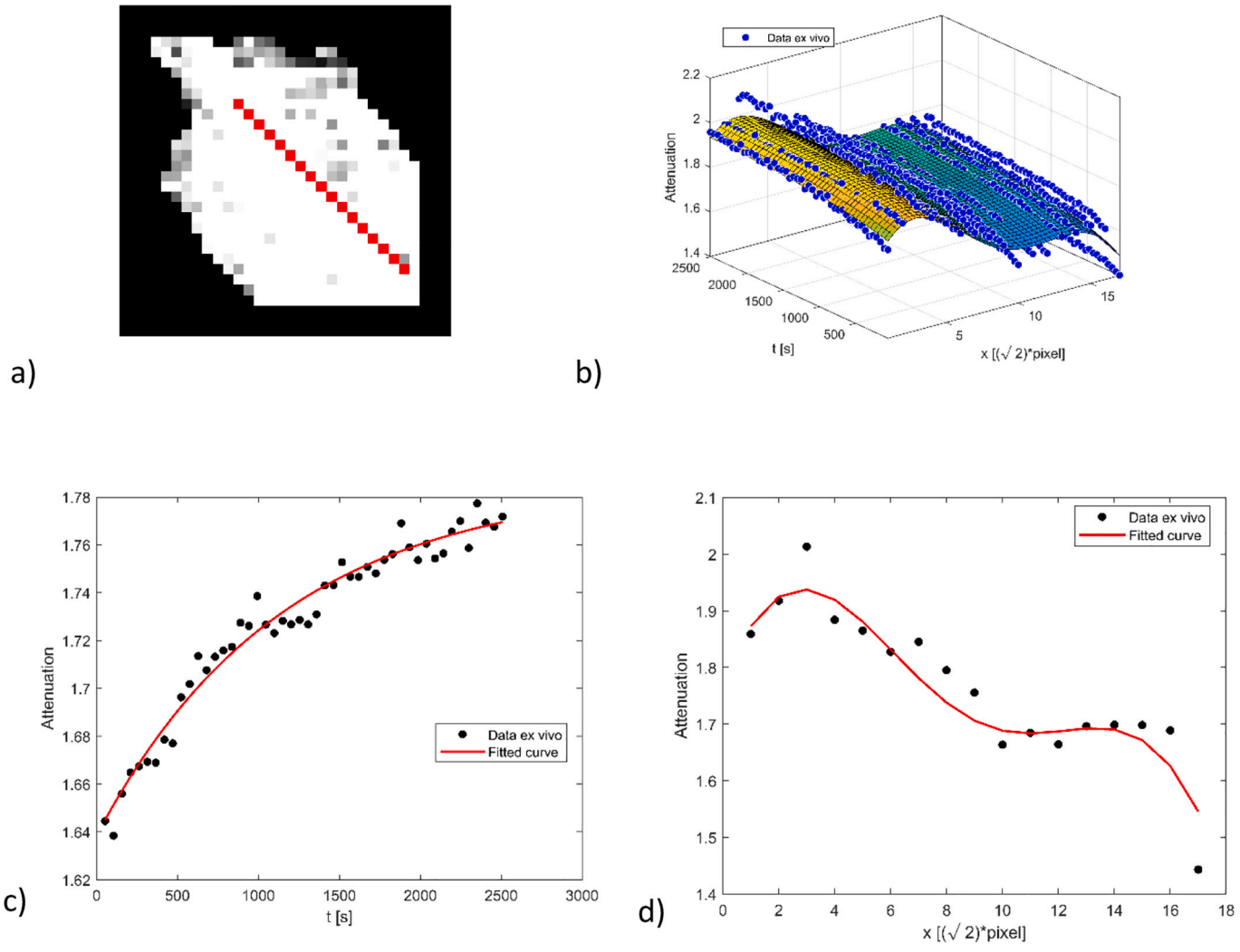

Fig. 5. a) Midvein middle section for y = 4. b) Fit in space and time. c) Data and fit extracted from b) *versus* time. d) Data and fit extracted from b) *versus* x.

Table 3
Fitting parameters (95% confidence bounds).

	C_0 (10^{-4})	C_1 (10^{-3})	C_2 (10^{-3})	k_b (10^{-4})	k_1 (10^{-3})	k_2 (10^{-2})	k_{chem} (10^{-4})	Δx	R^2
y1	3 ± 6	4 ± 1	70 ± 12	11 ± 5	38 ± 1	−96 ± 2	11 ± 5	116 ± 3	0.46
y2	33 ± 20	2 ± 2	12 ± 4	10 ± 4	14 ± 2	35 ± 2	4 ± 4	98 ± 7	0.53
y3	7 ± 4	18 ± 2	24 ± 4	11 ± 4	89 ± 6	26 ± 2	9 ± 4	44 ± 3	0.67
y4	4 ± 2	25 ± 1	39 ± 3	9 ± 3	107 ± 3	31 ± 1	7 ± 3	36 ± 1	0.86
y5	4 ± 2	84 ± 4	108 ± 7	9 ± 5	168 ± 4	28 ± 1	8 ± 4	20 ± 1	0.84
y6	2 ± 2	11 ± 1	59 ± 6	7 ± 5	80 ± 2	54 ± 1	6 ± 5	52 ± 1	0.77
y7	0.1 ± 1	37 ± 1	90 ± 6	5 ± 6	146 ± 2	44 ± 1	6 ± 6	24 ± 1	0.81

95% confidence bounds are reported in the Supplementary Information. Fig. 5a shows one of the lines (y = 4) where the midvein was divided for performing fits and the corresponding fitting results are reported in Table 3. Fig. 5b shows the plot of data *versus* time and space, while Fig. 5c and d show an example of the temporal and spatial behaviour extracted from Fig. 5b. As one can see, the fit reproduces the main features of the experimental points. In particular, the time dependence can be represented as an exponential growth, similarly to what was observed in the previous section.

The parameters C_0 and Δx can be considered to be related to the number of water molecules at the stalk cut and to the distance between the beginning of the midvein and the stalk cut, respectively. C_0 and Δx both tend to decrease moving towards higher y. The variation of C_0 and Δx with y can be related to the not perfect perpendicularity of the cut section with respect to the midvein axis: moving towards higher y the sections presumably present fewer water molecules. In those sections the value of C_0 would thus be lower just because Δx is lower and the water molecules coming from the liquid water in the syringe could be swallowed up more rapidly in the leaf midvein.

Following Eq. (4), C_1 and C_2 could be considered related to the average decrease in the number of water molecules in the midvein compared to the initial value, C_0. Both C_1 and C_2 increase proceeding towards higher y: following the discussion regarding C_0 and Δx, it can be assumed that the midvein section that is least distant from the cut of the stalk manages to swallow up more water molecules than the others, due to the smaller distance from liquid water in the syringe. Similarly, k_1 and k_2 can be considered related to the oscillation of water flow in the midvein; k_1 increases moving towards higher y: higher k_1 means faster oscillations, and following the discussion regarding C_1 and C_2, it can be assumed that the water flow oscillates faster as more water molecules are swallowed up in the midvein from the stalk cut. The values of k_b do not change significantly as one moves towards higher y and are in agreement with the k_b value of the *ex vivo* hydration fit in table 1.

These findings suggest that the method described above correctly reproduces the main features of the experimental results and can, therefore, be considered a reasonable model for this type of systems. This may pave the way for a more quantitative investigation on the managements of water from leaves under normal and stressed conditions and may also lead to important achievements for the next-generation precision biosensing. Moreover, it is potentially applicable to other biological systems, as well.

4. Conclusion

The attenuation in the terahertz range was monitored through a terahertz portable imaging system to reveal the hydration and dehydration dynamics of leaves both in *ex vivo* and *in vivo* leaves; the results were described with an exponential behaviour.

Moreover, the spatiotemporal dynamics of water diffusion were observed in an *ex vivo* leaf. A model was proposed starting from approximate solutions of diffusion law, gaining physical information from surface fits. A case study was chosen as an example and fits of the spatial and temporal behaviour of the hydration dynamics of a leaf were performed, implying that the interpretation of terahertz data in terms of water concentration derived from the solution of diffusion law is reasonable.

These results suggest that terahertz-based techniques and, in particular, imaging techniques, may represent very powerful methods to obtain meaningful *in vivo* information in real time. This may be also useful for a deeper insight into the biological samples water management behaviour with possible applications for the early detection of diseases in future precision biosensing and in several other fields.

CRediT authorship contribution statement

F.V. Di Girolamo: Conceptualization, Data curation, Formal analysis, Investigation, Methodology, Software, Writing – original draft, Writing – review & editing. **R. Paoletti:** Conceptualization, Funding acquisition, Methodology, Writing – review & editing, Supervision. **A. Tredicucci:** Conceptualization, Funding acquisition, Methodology, Supervision, Writing – review & editing. **A. Toncelli:** Conceptualization, Data curation, Investigation, Methodology, Supervision, Writing – original draft, Writing – review & editing.

Declaration of competing interest

The authors declare that they have no known competing financial interests or personal relationships that could have appeared to influence the work reported in this paper.

Data availability

Data will be made available on request.

Acknowledgments

We acknowledge the support from the project PRA_2022_2023_98 (“IMAGINATION”) from the University of Pisa and Sensorsek Project supported by the Italian Tuscany Government, POR FSE 2014 -2020, through the INFN-RT2 172800 Project.

References

[1] A. Bobard, N. Mellouk, J. Enninga, Spotting the right location—imaging approaches to resolve the intracellular localization of invasive pathogens, Biochim. Biophys. Acta Gen. Subj. 1810 (2011) 297.
[2] X. Yang, D. Wei, S. Yan, Y. Liu, S. Yu, M. Zhang, Z. Yang, X. Zhu, Q. Huang, H.-L. Cui, W. Fu, Rapid and label-free detection and assessment of bacteria by terahertz time-domain spectroscopy, J. Biophotonics 9 (2016) 1050.
[3] X. Yang, K. Yang, X. Zhao, Z. Lin, Z. Liu, S. Luo, Y. Zhang, Y. Wang, W. Fu, Terahertz spectroscopy for the isothermal detection of bacterial DNA by magnetic bead-based rolling circle amplification, Analyst 142 (2017) 4661.
[4] L. Yu, L. Hao, T. Meiqiong, H. Jiaoqi, L. Wei, D. Jinying, C. Xueping, F. Weiling, Z. Yang, The medical application of terahertz technology in non-invasive detection of cells and tissues: opportunities and challenges, RSC Adv. 9 (2019) 9354.
[5] F.V. Di Girolamo, A. Toncelli, A. Tredicucci, M. Bitossi, R. Paoletti, Leaf water diffusion dynamics in vivo through a sub-terahertz portable imaging system, J. Phys. Conf. Ser. 1548 (2020) 012002.
[6] F.V. Di Girolamo, M. Pagano, A. Tredicucci, M. Bitossi, R. Paoletti, G.P. Barzanti, C. Benvenuti, P.F. Roversi, A. Toncelli, Detection of fungal infections in chestunuts: a terahertz imaging based approach, Food Control 123 (2021) 107700.
[7] S.S. Dhillon, M.S. Vitiello, E.H. Linfield, A.G. Davies, C. Hoffmann, J. Booske, C. Paoloni, M. Gensch, P. Weightman, G.P. Williams, E. Castro-Camus, D.R. S. Cumming, F. Simoens, I. Escorcia-Carranza, J. Grant, S. Lucyszyn, M. Kuwata-Gonokami, K. Konishi, M. Koch, C.A. Schmuttenmaer, T.L. Cocker, R. Huber, A.

G. Markelz, Z.D. Taylor, V.P. Wallace, J. Axel Zeitler, J. Sibik, T.M. Korter, B. Ellison, S. Rea, P. Goldsmith, K.B. Cooper, R. Appleby, D. Pardo, P.G. Huggard, V. Krozer, H. Shams, M. Fice, C. Renaud, A. Seeds, A. Stöhr, M. Naftaly, N. Ridler, R. Clarke, J.E. Cunningham, M.B. Johnston, The 2017 Terahertz science and technology roadmap, J. Phys. D Appl. Phys. 50 (2017) 043001.

[8] S.L. Dexheimer (Ed.), Terahertz Spectroscopy: Principles and Applications, CRC Press, Taylor and Francis Group, 2008.

[9] H.B. Zhang, K. Mitobe, N. Yoshimura, Application of terahertz imaging to water content measurement, Jpn. J. Appl. Phys. 47 (2008) 8065.

[10] D.F. Alves-Lima, R. Letizia, R. Degl'Innocenti, R. Dawson, H. Lin, Quantitative video-rate hydration imaging of Nafion proton exchange membranes with terahertz radiation, J. Power Sources 450 (2020) 227665, https://doi.org/10.1016/j.jpowsour.2019.227665.

[11] A. Dobroiu, Masatsugu Yamashita, Yuichi N. Ohshima, Yasuyuki Morita, Chiko Otani, Kodo Kawase, Terahertz imaging system based on a backward-wave oscillator, Appl. Optics 43 (2004) 5637.

[12] E. Castro-Camus, M. Palomar, A.A. Covarrubias, Leaf water dynamics of Arabidopsis thaliana monitored in-vivo using terahertz time-domain spectroscopy, Sci. Rep. 3 (2013) 2910.

[13] R. Gente, M. Koch, Monitoring leaf water content with THz and sub-THz waves, Plant Methods 11 (2015) 15.

[14] U. Siciliani de Cumis, J.-H. Xu, L. Masini, R. Degl'Innocenti, P. Pingue, F. Beltram, A. Tredicucci, M.S. Vitiello, P.A. Benedetti, H.E. Beere, D.A. Ritchie, Terahertz confocal microscopy with a quantum cascade laser source, Opt. Express 20 (2012) 21924.

[15] L. Baldacci, M. Pagano, L. Masini, A. Toncelli, G. Carelli, P. Storchi, A. Tredicucci, Non-invasive absolute measurement of leaf water content using terahertz quantum cascade lasers, Plant Methods 13 (2017) 51, https://doi.org/10.1186/s13007-017-0197-z.

[16] M. Pagano, L. Baldacci, A. Ottomaniello, G. de Dato, F. Chianucci, L. Masini, G. Carelli, A. Toncelli, P. Storchi, A. Tredicucci, P. Corona, THz water transmittance and leaf surface area: an effective nondestructive method for determining leaf water content, Sensors 19 (2019) 4838, https://doi.org/10.3390/s19224838.

[17] R. Gente, N. Born, N. Voß, W. Sannemann, J. Leon, M. Koch, E. Castro-Camus, Determination of leaf water content from terahertz time-domain spectroscopic data, Journal of Infrared, Millimeter and Terahertz Waves 34 (2013) 316.

[18] B. Breitenstein, M. Scheller, M.K. Shakfa, T. Kinder, T. Müller-Wirts, M. Koch, D. Selmar, Introducing terahertz technology into plant biology: A novel method to monitor changes in leaf water status, J. Appl. Bot. Food Qual. 84 (2011) 15.

[19] F. Qu, P. Nie, L. Lin, C. Cai, Y. He, Review of theoretical methods and research aspects for detecting leaf water content using terahertz spectroscopy and imaging, International Journal of Agricultural and Biological Engineering 11 (2018) 27.

[20] S. Hadjiloucas, L.S. Karatzas, W.J. Bowen, Measurement of leaf water content using terahertz radiation, IEEE Transactions on Microwave Theory and Tecnology 47 (1999) 142.

[21] R. Li, Y. Lu, J.M.R. Peters, B. Choat, A.J. Lee, Non-invasive measurement of leaf water content and pressure-volume curves using terahertz radiation, Sci. Rep. 10 (2020) 21028.

[22] G.A. Beattie, Plant science: A war over water when bacteria invade leaves, Nature 539 (2016) 506.

[23] X. Chen, H. Lindley-Hatcher, R.I. Stantchev, J. Wang, K. Li, A. Hernandez Serrano, Z.D. Taylor, E. Castro-Camus, E. Pickwell-McPherson, Terahertz (THz) biophotonics technology: instrumentation, techniques, and biomedical applications, 2024.

[24] P. Atkins, J. De Paula, in: P. Atkins, J. De Paula (Eds.), Chimica Fisica, Zanichelli, fourth italian edition of the seventh american edition Atkin's Physical Chemistry, Seventh edition, Oxford University Press, 2002.

[25] Metodi Matematici della Fisica, C. Bernardini, O. Ragnisco, P.M. Santini, Carrocci editore (seconda ristampa, Maggio 2014), 2014.

[26] D.M. Kim, H. Zhang, H. Zhou, T. Du, Q. Wu, T.C. Mockler, M.Y. Berezin, Highly sensitive image-derived indices of water-stressed plants using hyperspectral imaging in SWIR and histogram analysis, Sci. Rep. 5 (2015) 15919.

[27] T. Kinder, T. Müller-Wirts, B. Breitenstein, D. Selmar, M. Schwerdtfeger, M. Scheller, et al., In-vivo-messung des blattwassergehalts mit terahertz-strahlung, BioPhotonik 1 (40) (2012) 2.

[28] H. Lambers, T.L. Pons, C F Stuart III, Plant Physiological Ecology, Springer, 2008.

[29] A.J. McElrone, B. Choat, G.A. Gambetta, C.R. Brodersen, Water uptake and transport in vascular plants, Nature Education Knowledge 4 (2013) 6.

[30] H.T. Nguyen, P. Meir, J. Wolfe, M. Mencuccini, M.C. Ball, Plumbing the depths: extracellular water storage in specialized leaf structures and its functional expression in a three-domain pressure–volume relationship, Plant, Cell Environ. 40 (2017) 1021.

[31] Z. Song, S. Yan, Z. Zang, Temporal and spatial variability of water status in plant leaves by terahertz imaging, IEEE Transactions on Terahertz Scientific Technology 8 (2018) 520.

[32] H. Zhou, G. Zhou, Q. He, L. Zhou, Y. Ji, X. Lv, Capability of leaf water content and its threshold values in reflection of soil-plant water status in maize during prolonged drought, Ecol. Indic. 124 (2021) 107395.